THE JOURNAL OF BIOLOGICAL CHEMISTRY VOL. 286, NO. 6, pp. 4632–4643, February 11, 2011

Cytochrome P450 7A1 Cholesterol 7α-Hydroxylation

INDIVIDUAL REACTION STEPS IN THE CATALYTIC CYCLE AND RATE-LIMITING FERRIC IRON REDUCTION[*][S]

Received for publication, October 11, 2010, and in revised form, December 6, 2010 Published, JBC Papers in Press, December 8, 2010, DOI 10.1074/jbc.M110.193409

Raku Shinkyo and F. Peter Guengerich[1]

From the Department of Biochemistry and Center in Molecular Toxicology, Vanderbilt University School of Medicine, Nashville, Tennessee 37232-0146

Cytochrome P450 (P450) 7A1 is well known as the cholesterol 7α-hydroxylase, the first enzyme involved in bile acid synthesis from cholesterol. The human enzyme has been reported to have the highest catalytic activity of any mammalian P450. Analyses of individual steps of cholesterol 7α-hydroxylation reaction revealed several characteristics of this reaction: (i) two-step binding of cholesterol to ferric P450, with an apparent K_d of 0.51 μM, (ii) a rapid reduction rate in the presence of cholesterol (~10 s^{-1} for the fast phase), (iii) rapid formation of a ferrous P450-cholesterol-O_2 complex (29 s^{-1}), (iv) the lack of a non-competitive kinetic deuterium isotope effect, (v) the lack of a kinetic burst, and (vi) the lack of a deuterium isotope effect when the reaction was initiated with the ferrous P450-cholesterol complex. A minimum kinetic model was developed and is consistent with all of the observed phenomena and the rates of cholesterol 7α-hydroxylation and H_2O and H_2O_2 formation. The results indicate that the first electron transfer step, although rapid, becomes rate-limiting in the overall P450 7A1 reaction. This is a different phenomenon compared with other P450s that have much lower rates of catalysis, attributed to the much more efficient substrate oxidation steps in this reaction.

Cytochromes P450 (P450)[2] enzymes are hemoproteins and most commonly catalyze oxidation reactions (Fig. 1) (3, 4). In mammals, P450 enzymes play important roles in the metabolism of both endogenous substrates (*e.g.* fatty acids, steroids, eicosanoids) and exogenous substrates (*e.g.* drugs, carcinogens, pesticides). Most mammalian P450 enzymes, especially the "drug-metabolizing" P450 enzymes (*e.g.* P450s 1A2, 2C9, 2D6), show relatively low catalytic activity ($k_{cat} < 10$ min^{-1}, often ~1 min^{-1}) (3–5) compared with some of the classical microbial P450 enzymes with high activities, *e.g.* P450s 101A1, 102A1 ($k_{cat} > 10^3$ min^{-1}) (5). On the other hand, a few mammalian P450 enzymes, *e.g.* rat P450 2B1 and 4A1, rabbit P450 4A7, and human P450 7A1, have been reported to have higher catalytic activities ($k_{cat} \geq 50$ min^{-1}) (6–9).

Among these latter mammalian P450s, P450 7A1 has been reported to have quite high catalytic activity toward the substrate cholesterol (as high as 5.8 s^{-1}) (9). This enzyme is well known as the cholesterol 7α-hydroxylase, the first and rate-limiting enzyme in the classic pathway of bile acid synthesis, with a daily elimination of 400–600 mg of cholesterol in humans (10, 11). A k_{cat}/K_m value reported for recombinant P450 7A1 was 4×10^5 M^{-1} s^{-1}, although the cholesterol 7α-hydroxylation activity in human liver microsomes has been reported to be <0.13 pmol/s/mg of microsomal protein (k_{cat} ~ 0.06 s^{-1}) (12–14). This efficiency (k_{cat}/K_m) of cholesterol 7α-hydroxylation by recombinant P450 7A1 is ~10-fold higher than that of testosterone 6β-hydroxylation by P450 3A4, which is one of the faster reactions catalyzed by the drug-metabolizing P450 enzymes (15). However, to our knowledge no detailed kinetic studies on cholesterol 7α-hydroxylation activity by P450 7A1 are available, and why P450 7A1 shows such high catalytic activity is unknown.

We have been interested in the reaction cycles of several mammalian P450s with low catalytic efficiencies, including the rate-limiting steps in reactions (15–18). Our previous reports on the reactions of P450s 1A2, 2A6, 2D6, and 3A4 show that the C-H bond-breaking step of each reaction is mainly or partially rate-limiting, as judged by kinetic deuterium isotope effects. Kinetic analysis on P450 7A1, with its high catalytic efficiency, was done for comparison with low efficiency P450 reactions to better understand differences between them and to define why P450 rates vary so much.

In the present study we analyzed individual reaction steps and developed a detailed kinetic model of P450 7A1 reaction cycle with individual rate constants. The substrate binding, C-H bond-breaking, and product release steps are not rate-limiting. The results indicate that the first electron transfer step, although as rapid as observed with other mammalian P450s, becomes rate-limiting in the P450 7A1 reaction.

EXPERIMENTAL PROCEDURES

Chemicals—Cholesterol, 17α-ethynylestradiol, dansyl chloride, 4,4-dimethylaminopyridine, protocatechuate, protocatechuate dioxygenase, HPβCD, and Tween 20 were purchased from Sigma. 7α-OH cholesterol was purchased from Steraloids (Newport, RI). HPLC grade solvents were purchased

* This work was supported, in whole or in part, by National Institutes of Health Grants R37 CA090426 and P30 ES000267 (to F. P. G.). This work was also supported by Eisai Co., Ltd. (to R. S.).

[S] The on-line version of this article (available at http://www.jbc.org) contains supplemental Figs. S1–S5.

[1] To whom correspondence should be addressed: Dept. of Biochemistry and Center in Molecular Toxicology, Vanderbilt University School of Medicine, 638 Robinson Research Bldg., 2200 Pierce Ave., Nashville, TN 37232-0146. Tel.: 615-322-2261; Fax: 615-322-3141; E-mail: f.guengerich@vanderbilt.edu.

[2] The abbreviations used are: P450, cytochrome P450; di-12:0 GPC, L-α-1,2-dilauroyl-*sn*-glycero-3-phosphocholine; 7α-OH cholesterol, 7α-hydroxycholesterol; HPβCD, 2-hydroxypropyl-β-cyclodextrin.

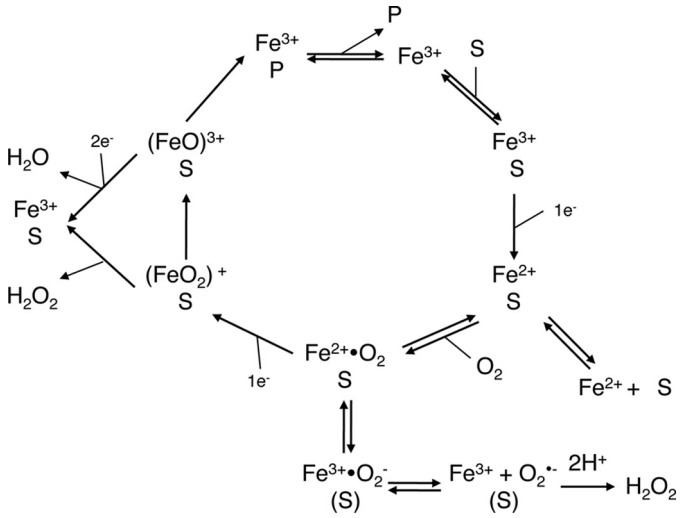

FIGURE 1. **P450 catalytic cycle (17).**

from Fisher. 5-Deazaflavin was a gift of the late V. Massey (University of Michigan, Ann Arbor, MI).

P450 7A1 Expression—An expression plasmid including the cDNA of truncated (Δ2–24) P450 7A1, with a C-terminal His_6 tag in pTrc 99a, was kindly provided by I. A. Pikuleva (Case Western Reserve University, Cleveland, OH) (9). This plasmid was transformed into *Escherichia coli* GC5-competent cells (Genesee Scientific Corp., San Diego, CA) with pGro7 (Takara, Shiga, Japan) and expressed as follows. An overnight culture was diluted 1:100 (v/v) into Terrific Broth medium (BD Diagnostics, Sparks, MD) containing ampicillin (0.3 mM) and chloramphenicol (0.5 mM) and grown at 37 °C with shaking at 250 rpm in an incubator (ATR Multitron, Laurel, MD) until the OD_{600} reached 0.6. Isopropyl 1-thio-β-D-galactopyranoside (1 mM), δ-aminolevulinic acid (0.5 mM), and L-arabinose (27 mM) were added, and the cultures were incubated at 26 °C for 42 h (190 rpm).

P450 7A1 Purification—All steps were performed at 4 °C. Cells were lysed, and a cytosolic fraction was obtained using modifications of a procedure reported previously (9). After dilution with Buffer A (400 mM potassium phosphate buffer (pH 7.2) containing 1 M KCl, 20% glycerol (v/v), 0.5% CHAPS (w/v), and 1 mM imidazole) to a concentration of 2 mg/ml total protein (as determined by a bicinchoninic acid assay (BCA, Pierce)), the cytosolic material was loaded onto a Ni^{2+}-nitrilotriacetic acid resin column (2.5 × 6 cm, Qiagen, Valencia, CA) equilibrated with Buffer A. The column was washed with 20 column volumes of Buffer B (400 mM potassium phosphate buffer (pH 7.2) containing 1 M NaCl, 20% glycerol (v/v), 0.5% CHAPS (w/v), and 20 mM imidazole). P450 7A1 was then eluted with Buffer C (400 mM potassium phosphate buffer (pH 7.2) containing 1 M NaCl, 20% glycerol (v/v), 0.5% CHAPS (w/v), and 300 mM imidazole). The fractions showing absorbance at 417 nm were pooled, dialyzed overnight against 100 sample volumes of Buffer D (10 mM potassium phosphate buffer (pH 7.2) containing 20% glycerol (v/v) and 0.3% CHAPS (w/v)), and applied to a hydroxylapatite column (2.5 × 5 cm) equilibrated with Buffer D. The column was washed with 10 column volumes of Buffer D, and P450 7A1 was eluted with 400 ml of an increasing linear gradient of 10–400 mM potassium phosphate buffer (pH 7.2, including 20% glycerol (v/v) and 0.3% CHAPS (w/v)). After two dialyzes (12 h) against 100 sample volumes of 100 mM potassium phosphate buffer (pH 7.4) including 20% glycerol (v/v) and 1 mM EDTA, the purified P450 7A1 was stored at −70 °C.

The expression level of P450 7A1 was ~ 600 nmol/liter. Purified P450 7A1 (final yield ~250 nmol from 1 liter of bacteria) showed a single major band when analyzed for electrophoretic purity as well as typical P450 spectral properties (supplemental Figs. S1 and S2).

Other Enzyme Preparations—Rat NADPH-P450 reductase was expressed in *E. coli* and purified as described elsewhere (19).

Spectroscopy—NMR spectra were recorded using a Bruker 500-MHz spectrometer in the Vanderbilt facility (Bruker, Billerica, MA).

Mass spectra of synthesized compounds were acquired in the Vanderbilt facility using a Thermo LTQ instrument (ThermoFinnigan, Sunnydale, CA) equipped with a Waters Acquity UPLC system (Waters, Milford, MA). A Thermo-Finnigan TSQ Quantum mass spectrometer (ThermoFinnigan) connected to a Waters Acuity UPLC system was used for quantitation of dansylated compounds. UV-visible spectra were recorded with either an Aminco DW2/OLIS or a Cary14/OLIS spectrophotometer (On-Line Instrument Systems, Bogart, GA).

Stopped-flow UV-visible absorbance experiments were performed using an OLIS RSM-1000 instrument (On-Line Instrument Systems) as described previously (16, 17). Stopped-flow experiments were generally reported as the averages of four individual kinetic assays.

Synthesis of 7-[$^2H_2$]-Cholesterol—A general procedure (20) was used; Al^2HCl_2 was prepared by stirring $LiAl^2H_4$ (Sigma, 58 mg, 1.4 mmol, > 98% D atom excess) and $AlCl_3$ (0.73 g, 5.5 mmol) in dry $(C_2H_5)_2O$ (freshly opened can) for 10 min at −20 °C under dry N_2. To this was added (dropwise, in $(C_2H_5)_2O$) 184 mg of 7-ketocholesterol (Sigma, 0.46 mmol) over 10 min. The reaction was stirred for an additional 10 min and quenched with the careful addition of H_2O. The product was extracted into $(C_2H_5)_2O$ three times, and the combined layers were dried with $MgSO_4$ and concentrated *in vacuo*. The product was purified using isocratic reversed-phase HPLC with a Phenomenex octadecylsilane column (10 × 250 mm, 5 μm, Phenomenex, Torrance, CA). HPLC conditions were as follows. The solvent contained 45% CH_3CN, 50% CH_3OH, and 5% *tert*-butyl methyl ether (v/v/v), and the flow rate was 1.0 ml/min. The column temperature was maintained at 25 °C. The t_R of d_2-cholesterol was 32 min. LC-MS analysis indicated that the purified d_2-cholesterol had >98.5% isotopic purity (supplemental Fig. S3, *A* and *B*). The disappearance of the δ 1.97 ^1H NMR peak and the decrease in the number of integrated ^1H peaks located between δ 1.48 and 1.62 from 9 (d_0-cholesterol, supplemental Fig. S3*C*) to 8 (d_2-cholesterol, supplemental Fig. S3*D*) indicate that both the H-7α and H-7β atoms were substituted with deuterium (20–22). The singlet peak for the H-6 proton (δ 5.35) of d_2-choles-

terol is also indicative of the incorporation of deuterium atoms at both the 7α- and 7β-positions.

Measurement of Enzyme Activity with Reconstituted Enzyme Systems—Steady-state enzyme assays were generally conducted in a 0.50-ml reaction volume at 37 °C for 60 s in 50 mM potassium phosphate buffer (pH 7.4). Enzyme reaction mixtures typically contained 0.02 μM P450 7A1, 1.0 μM NADPH-P450 reductase, 60 μM di-12:0 GPC, 3.1 mM HPβCD (0.45%, w/v)), and 0.41 mM Tween 20 (0.05%, v/v)). Incubations were initiated by the addition of an NADPH-generating system (23). Reactions were quenched with 2.0 ml of CH_2Cl_2 including 150 pmol of 17α-ethynylestradiol (as an internal standard) and mixed with a vortex device. After centrifugation (2000 $\times$ *g*, 5 min), 1.4 ml of the organic layer was transferred and taken to dryness under an N_2 stream. A general method for derivatization with dansyl chloride (24) was used with slight modification. Briefly, the samples were dissolved in 200 μl of CH_2Cl_2 containing 2 mg of dansyl chloride, 0.5 mg of 4,4-dimethylaminopyridine, and 2 μl of triethylamine and incubated at 65 °C for 1 h. The samples were dried under an N_2 stream and then dissolved in 100 μl of CH_3CN for analysis.

Dansylated products were analyzed with LC-MS using a UPLC system connected to a TSQ Quantum mass spectrometer with a Hypersil GOLD octadecylsilane column (2.1 $\times$ 150 mm, 3 μm, Thermo Scientific). LC conditions were as follows. Solvent A contained 95% H_2O, 5% CH_3CN, and 0.1% HCO_2H (v/v/v), and solvent B contained 5% H_2O, 85% CH_3CN, 10% *tert*-butyl methyl ether, and 0.1% HCO_2H (v/v/v/v). The column was maintained at the initial condition of 50% B (v/v) for 0.5 min with a flow rate of 350 μl/min followed by a linear gradient increasing to 100% B over 2.0 min. This condition was maintained for 6.5 min and then returned to the initial condition over 0.05 min and maintained until the end of a 12-min run. The column temperature was maintained at 40 °C. The injection volume (onto the column) was 15 μl. MS analyses were performed in the positive ion electrospray mode. Quantitation was done in a multiple reaction monitoring mode (dansylated 7α-OH cholesterol, *m*/*z* 636 $\rightarrow$ 367, collision energy 10 V; dansylated 17α-ethynylestradiol, *m*/*z* 530 $\rightarrow$ 171, collision energy 40 V). The following (optimized) parameters were used for the detection of the analyte and the internal standard; N_2 sheath gas, 27 p.s.i.; N_2 auxiliary gas, 25 p.s.i.; spray voltage, 5.0 kV; capillary temperature, 270 °C; capillary offset, 35 V; tube lens voltage, 221 V; argon collision gas, 1.5 mtorr; scan time, 50 ms Q3 scan width 1 *m*/*z*; Q1/Q3 peak widths at half-maximum, 0.7 *m*/*z*. The data were collected and quantified using ThermoFinnigan XCalibur Version 1.0 software.

Kinetic deuterium isotope effects were determined using a non-competitive method. P450 7A1 was incubated with either d_0-cholesterol or 7,7-d_2-cholesterol, varying the concentration from 0.625 to 20 μM in the general reconstituted system. The k_{cat} and K_m values were calculated using the program Dynafit (25). The product formed from 7,7-d_2-cholesterol by P450 7A1 was 7β-d_1,7α-OH cholesterol (26) (see below). Dansylated 7β-d_1,7α-OH cholesterol was quantified in the multiple reaction monitoring method, monitoring at *m*/*z* 637 $\rightarrow$ 368, assuming that the ion intensity of dansylated 7β-d_1,7α-OH cholesterol is the same as that of dansylated 7α-OH cholesterol.

Pre-steady-state rapid quench kinetic experiments were conducted with a quenched-flow apparatus (model RFQ-3, KinTek Corp., Austin, TX). Enzyme reaction mixtures contained 0.5 μM P450 7A1, 7.5 μM NADPH-P450 reductase, 60 μM di-12:0 GPC, 50 μM cholesterol, 3.1 mM HPβCD, and 0.41 mM Tween 20. Incubations were initiated by the rapid addition of 500 μM NADPH and quenched by the addition of 2% $ZnSO_4$ (w/v) after a time period varying from 20 ms to 2 s at 37 °C. After extraction, the derivatization and quantitation steps were conducted as described above.

Rates of NADPH Oxidation and H_2O_2 and H_2O Formation—NADPH oxidation and H_2O_2 and H_2O formation were measured as described previously (18). These experiments were conducted with a reconstituted system described above using 200 μM NADPH instead of an NADPH-generating system.

Anaerobic Experiments—The basic system is as described previously (16, 17), with a protocatechuate/protocatechuate dioxygenase oxygen-scrubbing system used in the reduction studies and the cholesterol binding study with the ferrous form of P450 7A1 (27). The scrubbing system was not used in the reactions of ferrous P450 7A1 with oxygen.

Kinetic Analyses and Modeling—The program Dynafit (25) was used for fitting of steady-state binding and activity data and the P450 reaction model. KinTek Explorer® software (KinTek Corp., Austin, TX) (28) was used for pre-steady-state binding studies. GraphPad Prism (GraphPad, San Diego, CA) was employed for fitting other data.

Kinetic Deuterium Isotope Effect Study with Human Liver Microsomes—The amount of cholesterol in human liver microsomal samples was first quantified. Human liver microsomes were diluted with H_2O (0.01 mg protein/ml), and 1.0 ml of each diluted sample was extracted with 2.0 ml of CH_2Cl_2, including 1.0 nmol of 7α-OH cholesterol (as the internal standard). After centrifugation, 1.4 ml of the organic layer was transferred, dried under an N_2 stream, and dissolved in 200 μl of CH_2Cl_2 containing 2 mg of dansyl chloride, 0.5 mg of 4,4-dimethylaminopyridine, and 2 μl of triethylamine and incubated at 65 °C for 1 h (24). The samples were dried under an N_2 stream and then dissolved in 75 μl of CH_3OH for analysis.

Dansylated products were analyzed with a UPLC system connected to an Acquity fluorescence detector using an Acquity UPLC BEH C18 octadecylsilane column (2.1 $\times$ 50 mm, 1.7 μm, Waters). LC conditions were as follows. Solvent A contained 95% H_2O, 5% CH_3CN, and 0.1% HCO_2H (v/v/v), and solvent B contained 5% H_2O, 85% CH_3CN, 10% *tert*-butyl methyl ether, and 0.1% HCO_2H (v/v/v/v). The column was maintained at the initial condition of 50% B (v/v) for 0.25 min with a flow rate of 500 μl/min followed by a linear gradient increasing to 100% B over 1.0 min. This condition was maintained for 4.25 min then returned to the initial condition over 0.01 min and maintained until the end of a 7-min run. The column temperature was maintained at 40 °C. The injection volume was 7.5 μl. Fluorescence measurements were made

using an excitation wavelength of 340 nm and an emission wavelength of 525 nm. The data collection and quantitative analysis were conducted with Waters MassLynx version 4.1 and QuanLinx Version 4.1 software, respectively.

Aliquots of individual human liver microsomes including exactly 10 nmol of cholesterol were added to a 0.50-ml of reaction mixture contained 3.1 mM HPβCD in 50 mM potassium phosphate buffer (pH 7.4). The assays were conducted at 37 °C for 30 min. Incubations were initiated by the addition of an NADPH-generating system. After extraction, the derivatization and quantitation steps were conducted as described above.

Immunoquantitation of P450 7A1 in Human Liver Microsomes—The proteins in individual human liver microsomes (75 μg of protein per well, in triplicate) were separated by sodium dodecyl sulfate-polyacrylamide gel electrophoresis (7.5%, w/v) along with standard samples that included 75 μg of human liver microsomal protein and varying amounts of purified P450 7A1 (0–600 fmol) per well. The proteins were electrophoretically transferred to a polyvinylidene fluoride membrane (Bio-Rad). A commercial primary rabbit polyclonal antibody to human P450 7A1 (ab79847, Abcam, Cambridge, UK) was used (1500-fold dilution in 10 mM potassium phosphate buffer (pH 7.4 containing 150 mM NaCl)). The secondary antibody was goat anti-rabbit IRD800CW, which emits infrared light at 800 nm (detected using an Odyssey Li-Cor instrument (Li-Cor, Lincoln, NE)). The slope of the standard curve (based on the spiked samples) was used to quantify the amount of P450 7A1 in individual human liver microsomal samples.

RESULTS

Cholesterol 7α-Hydroxylation Activity of P450 7A1—The rates of cholesterol 7α-hydroxylation activity of P450 7A1 measured in the presence of 0.41 mM Tween 20 were more than 6-fold higher than those measured in the absence of Tween 20 (Fig. 2*A*). This result confirmed that Tween 20 is essential for the high catalytic activity under these experimental conditions, as reported previously (29, 30). Cholesterol binding to Tween 20 and HPβCD has been reported with K_d values of 2.5 and 1.5 mM, respectively (29), which were used here. All models used to fit the data in this report include these two equilibria (*i.e.* cholesterol + Tween 20 $\rightleftarrows$ cholesterol-Tween 20 and cholesterol + HPβCD $\rightleftarrows$ cholesterol-HPβCD), further assuming that k_{on} values of cholesterol for both compounds are $\sim 10^8$ M^{-1} s^{-1} (supplemental Fig. S4*A*).

The rate of cholesterol 7α-hydroxylation was dependent on the concentration of NADPH-P450 reductase (Fig. 2*B*), and with 0.20 μM P450 7A1 in the assay a 15-fold greater concentration of the reductase was required for saturation (*i.e.* 3 μM). When the experiment was repeated with 20 nM P450 7A1, the concentration of reductase required for saturation was 1000 nM (50-fold excess) (results not shown). The estimated K_d value of the NADPH-P450 reductase-P450 7A1 complex was estimated to be 1.2 ± 0.3 μM using a Dynafit analysis of three sets of data (P450 concentrations of 20, 200, and 500 nM P450 7A1), *i.e.* treating the reductase as a substrate and assuming that steps after binding are not limiting (somewhat over-simplified model). The calculated k_{cat} and K_m cholesterol values (in the presence of 0.41 mM Tween 20) were 3.1 ± 0.3 s^{-1} and 1.3 ± 0.4 μM, respectively (Fig. 2*A*, supplemental Fig. S4*A*), yielding an estimated catalytic efficiency of 2.4×10^6 M^{-1} s^{-1}.

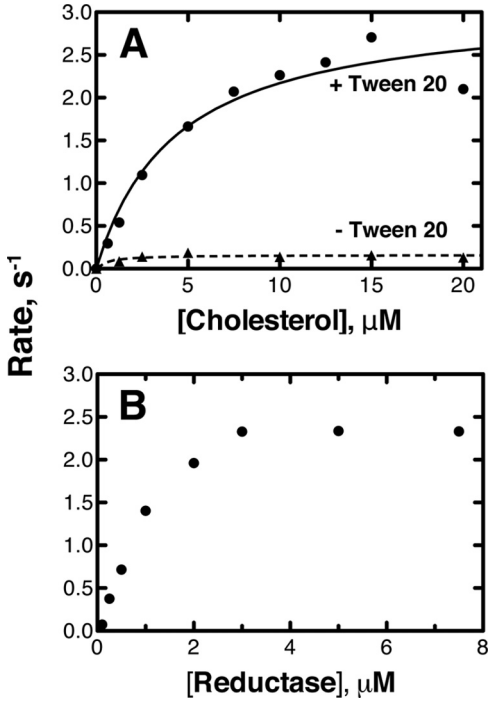

FIGURE 2. **Steady-state kinetics of P450 7A1 cholesterol 7α-hydroxylation.** *A*, data points are shown (●, with 0.41 mM Tween 20; ▲, the absence of Tween 20). The lines fitting results (Dynafit) of the formation of 7α-OH cholesterol by P450 7A1 in the presence (*solid*) and absence (*dashed*) of 0.41 mM Tween 20. *B*, dependence of the rate of cholesterol 7α-hydroxylation upon the concentration of NADPH-P450 reductase is shown shown. In *B* the P450 7A1 concentration was 0.20 μM, and the cholesterol concentration was 20 μM (with Tween 20 present). See supplemental Fig. S4 regarding fitting.

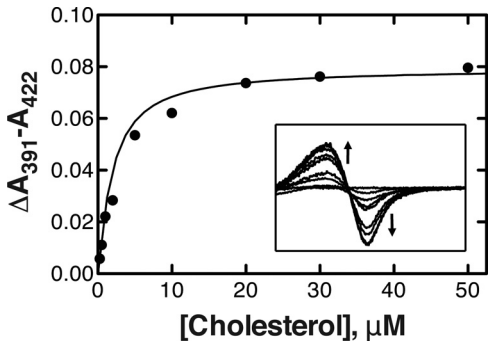

FIGURE 3. **Binding of cholesterol to P450 7A1.** Steady-state titration of 1.0 μM P450 7A1 was done with increasing concentrations of cholesterol in the presence of 3.1 mM HPβCD and 0.41 mM Tween 20. The plot (*line*) is a fit of the changes in absorbance (●) made using the program Dynafit. The *inset* shows the spectral changes. Parameters: $K_1 = 2.5 \times 10^{-3}$ M, $K_2 = 1.5 \times 10^{-3}$ M, $k_{+3} = 2.5 \times 10^7$ M^{-1} s^{-1}, $k_{-3} = 98$ s^{-1}, $k_{+4} = 18$ s^{-1}, $k_{-4} = 2.4$ s^{-1}. See supplemental Fig. S4 regarding fitting.

Steady-state and Pre-steady-state Kinetics of Cholesterol Binding to P450 7A1—Binding of cholesterol to P450 7A1 induced a substrate-type (type I) difference spectrum (31) (Fig. 3, *inset*). The rates of spectral changes were monitored using stopped-flow spectroscopy (Fig. 4). The traces could not be fit well to a simple one-step binding model (E + L $\rightleftarrows$ EL), even when including the steps of cholesterol binding to

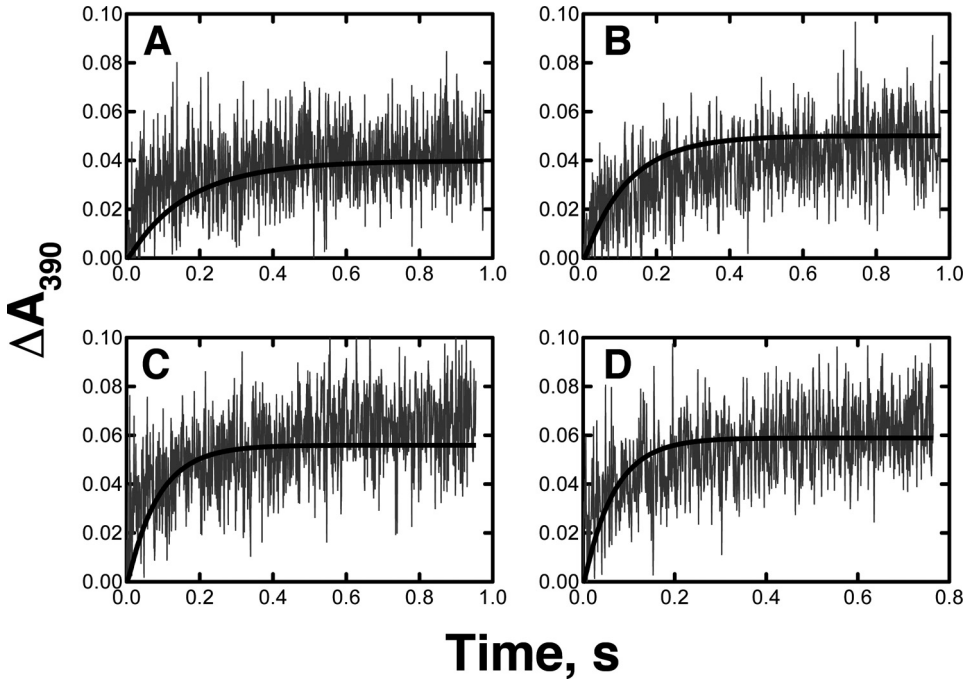

FIGURE 4. **Pre-steady-state binding kinetics of cholesterol to P450 7A1.** Stopped-flow absorbance changes (*A–D*, ΔA_{390}) are shown for binding of various concentrations (4, 8, 16, and 32 μM) of cholesterol to 2.0 μM P450 7A1 in the presence of 60 μM di-12:0 GPC, 3.1 mM HPβCD, and 0.41 mM Tween 20. Raw data are shown as *gray traces*, and the overlaid *black lines* are fitting results using KinTek Explorer® software. *A*, 4 μM cholesterol. *B*, 8 μM cholesterol. *C*, 16 μM cholesterol. *D*, 32 μM cholesterol. Parameters: $k_{+1} = 1.0 \times 10^8$ M^{-1} s^{-1}, $k_{-1} = 2.5 \times 10^5$ s^{-1}, $k_{+2} = 1.0 \times 10^8$ M^{-1} s^{-1}, $k_{-2} = 1.5 \times 10^5$ s^{-1}, $k_{+3} = 2.5 \times 10^7$ M^{-1} s^{-1}, $k_{-3} = 98$ s^{-1}, $k_{+4} = 18$ s^{-1}, $k_{-4} = 2.4$ s^{-1}. See supplemental Fig. S5 regarding fitting.

Tween 20 and HPβCD (see above) using KinTek Explorer® software, although the calculated k_{on} value, $2.3 \pm 0.2 \times 10^6$ M^{-1} s^{-1}, is acceptable as a diffusion-limited rate constant for interaction of an enzyme and ligand (32). Instead of a one-step model, a two-step binding model (E + L ⇄ EL ⇄ LE) was used, with a spectroscopically silent first step followed by a second conformational change step associated with the change in the spectrum of P450 7A1 (33–35) (supplemental Fig. S2). This two-step binding model provided a good fit to the curve, and the K_d value calculated from the rate constants was 0.51 μM (Fig. 4). This model, with the calculated rate constants, also provided a good fit to steady-state titration data, indicating that the model is reasonable for cholesterol binding to P450 7A1 (Fig. 3, supplemental Fig. S4*B*).

Ferric P450 7A1 Reduction Kinetics—The rate of CO binding to ferrous P450 7A1 was measured. One syringe contained 2.0 μM P450 7A1, 120 μM di-12:0 GPC, 40 μM cholesterol, 6.2 mM HPβCD, and 0.82 mM Tween 20 in 50 mM potassium phosphate buffer (pH 7.4, reduced with excess solid $Na_2S_2O_4$ immediately before loading), and the other syringe contained CO-saturated (nominally 1000 μM CO) 50 mM potassium phosphate buffer (pH 7.4). The rate of the binding of CO to P450 7A1 was estimated at 24 ± 1 s^{-1} using GraphPad Prism software (single exponential, data not shown). This CO binding step was incorporated into a model to estimate reduction rates of ferric P450 7A1 (see below).

Ferric P450 7A1 reduction rates were measured in an anaerobic CO environment, with ferrous P450 trapped as the CO complex. The rate of reduction of ferric P450 7A1 was slow in the absence of cholesterol, with a fit to a single exponential of 0.18 ± 0.01 s^{-1} (Fig. 5*D*). In the presence of cholesterol, the trace included fast and slow phases (Fig. 5*A*). Thus, the parts were fit separately, with $k_{fast} = 9.9 \pm 0.8$ s^{-1} and $k_{slow} = 0.10 \pm 0.01$ s^{-1}, corrected for the rate of CO binding (see above, Fig. 5, *B* and *C*, and supplemental Fig. S4*C*). About 60% of the P450 7A1 was reduced in the fast phase.

Cholesterol Binding to Ferrous P450 7A1—A difference spectrum between ferrous P450 7A1 and a ferrous P450 7A1-cholesterol complex was observed, with a trough at 435 nm and a weak peak at 480 nm (Fig. 6*A*, supplemental Fig. S2), similar to that reported for P450 2A6 (17). A titration of 1.0 μM P450 7A1 (reduced with excess $Na_2S_2O_4$) was done with increasing concentrations of cholesterol up to 50 μM (data not shown). The data were fit to a one-step binding model with a K_d value of 0.18 ± 0.03 μM using the program Dynafit. The rate of the change of absorbance at 438 nm was monitored using stopped-flow spectroscopy and could be fit to a single-exponential binding model (Fig. 6*B*). The rate constants for binding to ferrous P450 7A1 were $k_{+3} = 1.9 \times 10^6$ M^{-1} s^{-1} and (for dissociation) $k_{-3} = 0.30$ s^{-1} ($K_d = k_{-3}/k_{+3} = 0.16$ μM), consistent with the K_d value estimated by steady-state spectral analysis. Thus, the affinity of cholesterol for the ferric and ferrous forms of P450 7A1 appears to be similar.

Formation and Decomposition of Ferrous P450 7A1-O_2 Complex—A photo-reduced P450 7A1-cholesterol complex was loaded into one syringe of the stopped-flow spectrometer under an anaerobic environment (argon) and mixed with aerobic buffer (nominal final concentration 100 μM O_2). Rapid changes in the absorbance, particularly at 430 and 550 nm, were detected, in line with previous work with P450s 1A2 and 3A4 (16, 36, 37) (up to a reaction time of 160 ms, followed by a slower decrease (Fig. 7)). The rate for the first change in ab-

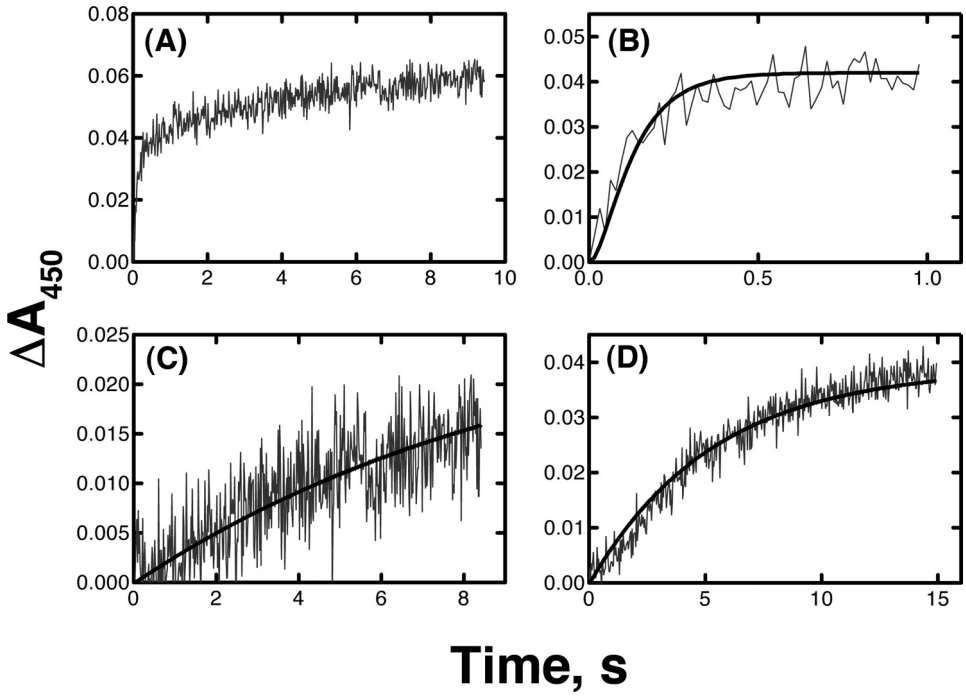

FIGURE 5. **Reduction kinetics of P450 7A1.** Stopped-flow absorbance changes of the reduction of 1.0 μM P450 7A1 by 2.0 μM NADPH-P450 reductase in the presence (*A–C*) and the absence (*D*) of 20 μM cholesterol upon the addition of 150 μM NADPH are shown. Raw data are shown as *gray traces*, and the overlaid *black lines* are fitting results (single exponential) obtained using the program Dynafit: with cholesterol (*B*, k_{fast} 9.9 ± 0.8 s^{-1}; C, k_{slow} 0.10 ± 0.01 s^{-1}) and without cholesterol (*D*, k = 0.18 ± 0.01 s^{-1}). See supplemental Fig. S4 regarding fitting.

sorbance was 29 s^{-1} (Fig. 7*C*, single-exponential) and is considered to be associated with the formation of a ferrous P450 7A1-O_2 complex. The rate for the second phase (decreased absorbance) was 1.2 s^{-1} (Fig. 7*B*, single-exponential). This decrease of absorbance is interpreted to be related to the decomposition of ferrous P450 7A1-O_2 complex to ferric P450 7A1 (Fig. 1).

Kinetic Deuterium Isotope Effects with P450 7A1 (Steady-state)—A non-competitive deuterium isotope experiment comparing the rates of 7α-hydroxylation of d_0- and d_2-cholesterol yielded $^{D}V = 0.94$ and $^{D}(V/K) = 1.15$ (with the parameters $^{H}k_{cat}$ = 3.1 ± 0.3 s^{-1}, $^{H}K_m$ = 1.3 ± 0.4 μM, $^{D}k_{cat}$ = 3.3 ± 0.2 s^{-1}, and $^{D}K_m$ = 1.6 ± 0.3 μM)[2] (Fig. 8 and Table 1).[3] The results clearly show the lack of a significant kinetic deuterium isotope effect for C-H bond breaking in steady-state cholesterol 7α-hydroxylation activity.

Because of the stereospecific nature of the hydroxylation, the intrinsic kinetic deuterium isotope effect (2) could not be estimated in a simple intramolecular experiment. However, we found that P450 3A4 catalyzed slow 7α- and 7β-hydroxylation of cholesterol with apparent isotope effects of 6.3 and 11, respectively, indicating that the C-H bond breaking step has an inherently high intrinsic kinetic isotope effect that is not expressed in the P450 7A1 reaction.[4]

Product Release from P450 7A1—Binding of 7α-OH cholesterol to P450 7A1 induced a type I difference spectrum, although the amplitude of the absorbance change was small. With the assumption that the K_d values of 7α-OH cholesterol with Tween 20 and HPβCD are similar to those for cholesterol (see above), the titration data fit to a one-step binding model with a K_d value of 3.7 ± 0.4 μM (Fig. 9).

No kinetic burst was observed in the P450 7A1 cholesterol 7α-hydroxylation reaction (Fig. 10). Therefore, this result indicates that any rate-limiting steps do not occur after product formation. Furthermore, in this experiment P450 7A1 was mixed with cholesterol in the initial reaction mixture; *i.e.* the P450 reaction cycle was started not from the free form of P450 7A1 but from a ferric P450 7A1-cholesterol complex (Fig. 1). This result also indicates that the substrate binding step cannot be a rate-limiting step in that linearity was observed beyond a stoichiometric formation of product (0.5 μM).

Formation of Product and Kinetic Deuterium Isotope Effects in Limited Turnover Experiments—Non-competitive deuterium isotope effects were examined when the P450 cycle was started from a Fe^{2+}-cholesterol complex, with modification of the approach used in Fig. 7. P450 7A1 (5 nmol) was either photo-reduced or reduced by NADPH-P450 reductase (5 nmol) under an argon atmosphere. In the cases in which the reductase was included, a limited amount of NADPH (12.5 nmol, *i.e.* enough to fully reduce the reductase and P450 for a single P450 cycle) was added. The reduction of ferric P450 7A1 was confirmed by monitoring the spectral changes. After reduction, the solutions were mixed with O_2 buffer, and the amount of product formed was measured (LC-MS).

7α-OH cholesterol was detected in the experiment with only (photo-reduced) P450 present (Table 2). As reported previously with other P450s (16, 17), the product must result

[3] For the kinetic deuterium isotope effects, the conventions of Northrop were used: ^{D}V, $^{H}k_{cat}/^{D}k_{cat}$; $^{D}(V/K)$, $(^{H}k_{cat}/^{H}K_m)/(^{D}k_{cat}/^{D}K_m)$ (1, 2).

[4] Experiments were done at a single cholesterol concentration of 100 μM for 10 min, and products were qualified using the dansylation procedure. The rates of formation of 7α- and 7β-hydroxycholesterol (from d_0-cholesterol) were 0.89 and 2.3 pmol/min/nmol of P450 3A4, respectively.

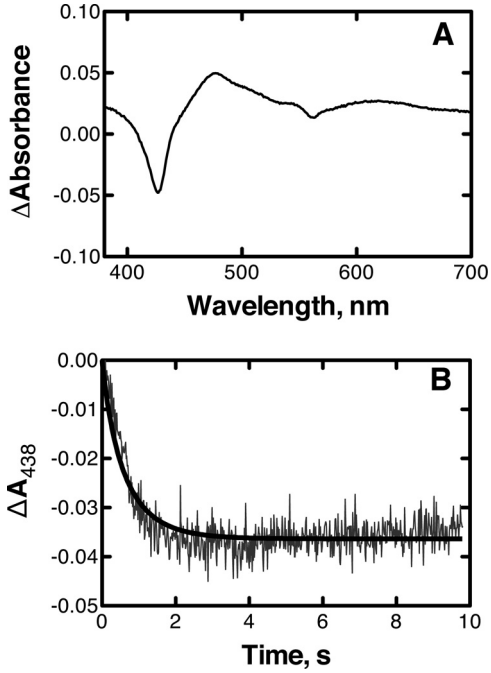

FIGURE 6. **Binding of cholesterol to ferrous P450 7A1.** *A*, shown is a difference spectrum obtained with 5.0 μM P450 7A1 with and without 30 μM cholesterol (in 50 mM potassium phosphate buffer (pH 7.4), including 3.1 mM HPβCD and 0.41 mM Tween 20). Both cuvettes were reduced with a few grains of $Na_2S_2O_4$. *B*, shown is a stopped-flow absorbance change (ΔA_{438}) for binding of cholesterol to ferrous (Fe^{2+}) P450. One syringe contained 4 μM cholesterol (in 50 mM potassium phosphate buffer (pH 7.4) including 3.1 mM HPβCD and 0.41 mM Tween 20), and the other contained 4.0 μM P450 7A1, 4.0 μM NADPH-P450 reductase, 120 μM di-12:0 GPC, 3.1 mM HPβCD, 0.41 mM Tween 20, and 50 μM NADPH in 50 mM potassium phosphate buffer (pH 7.4). Both syringes were anaerobic (argon). Raw data are shown as a *gray line*, and the *black line* was fit using KinTek Explorer® software. $k_{+1} = 1.0 \times 10^8\ M^{-1}\ s^{-1}$, $k_{-1} = 2.5 \times 10^5\ s^{-1}$, $k_{+2} = 1.0 \times 10^8\ M^{-1}\ s^{-1}$, $k_{-2} = 1.5 \times 10^5\ s^{-1}$, $k_{+3} = 1.9 \times 10^6\ M^{-1}\ s^{-1}$, $k_{-3} = 0.30\ s^{-1}$. See supplemental Fig. S5 regarding fitting.

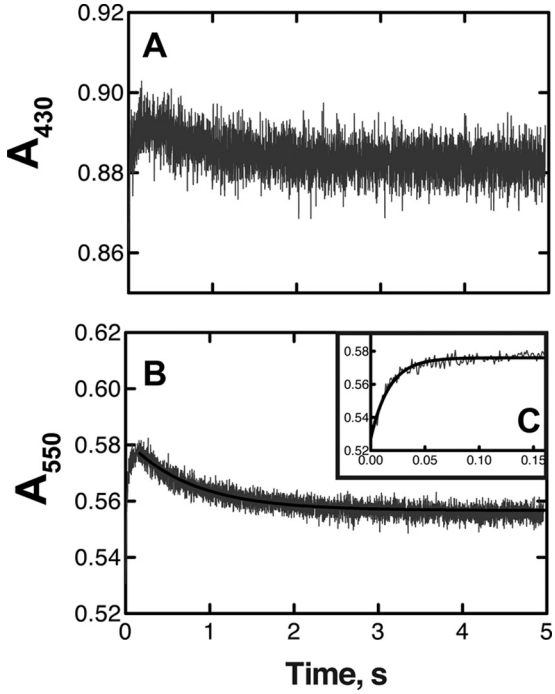

FIGURE 7. **Reaction of Ferrous P450 7A1 with O_2.** One syringe contained 4.0 μM P450 7A1, 120 μM di-12:0 GPC, 40 μM cholesterol, 3.1 mM HPβCD, 0.41 mM Tween 20, and 2 μM 5-deazaflavin in 50 mM potassium phosphate buffer (pH 7.4), and the other contained air-saturated 50 mM potassium phosphate buffer (pH 7.4), including 3.1 mM HPβCD and 0.41 mM Tween 20. Stopped-flow absorbance changes of cholesterol-bound ferrous P450 7A1 (photochemically reduced) after mixing with air-saturated buffer are shown. *C*, is an *inset* shows the first portion of A_{550} data. Raw data are shown as *gray traces*, and the overlaid *black lines* are fits (single exponential) using GraphPad Prism software. Parameters obtained from fits of the A_{550} data were used in subsequent fitting: *B*, $k = 1.2 \pm 0.1\ s^{-1}$; *C*, $k = 29 \pm 2\ s^{-1}$.

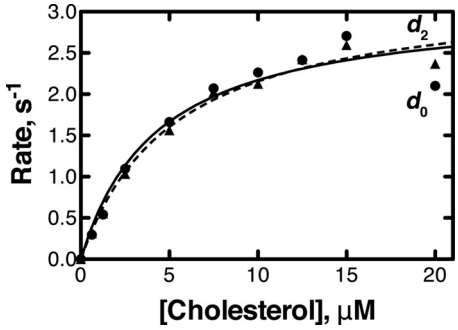

FIGURE 8. **Comparison of rates of d_0- and 7,7-d_2-cholesterol 7α-hydroxylation by P450 7A1.** Data points are shown (●, d_0-cholesterol; ▲, d_2-cholesterol). The lines (*solid line*, d_0-cholesterol; *dashed line*, d_2-cholesterol) are fits (hyperbolic plots) obtained using the program Dynafit. See Table 1 for parameters.

from the interaction of two Fe-O_2^{2+} complexes through the formation of Fe-O_2^{+} (*e.g.* 2 Fe-$O_2^{2+} \rightarrow FeO^{3+} + Fe^{3+} + O^{2-}$, $O^{2-} + 2H^+ \rightleftarrows H_2O$).

Product formation was more efficient when electrons were transferred from the reductase to P450, and the yield of d_1-7α-OH cholesterol in the system was similar to that for d_0-7α-OH cholesterol. A replicate experiment yielded a similar lack of a kinetic deuterium isotope effect. These results suggest that the rate of C-H bond breaking step is faster than the rates of O_2 binding, the second electron transfer, and the O_2 activation steps (Fig. 1).[5]

Stoichiometry of NADPH Utilization—Rates of NADPH oxidation, product formation, and H_2O_2 formation were measured at a single concentration of the substrate cholesterol (20 μM) (Table 3). The H_2O formation rate was calculated by difference (38). Under these experimental conditions, 65% of the NADPH that was oxidized was used to form the product 7α-OH cholesterol, which is a relatively high value compared with other microsomal P450s (17, 33, 36). These data were used in the kinetic modeling (see below).

TABLE 1

Kinetic deuterium isotope effect on 7α-hydroxylation activity of P450 7A1 (see Fig. 8)

Substrate	k_{cat}	K_m	^DV	$^D(V/K)$
	s^{-1}	μM		
d_0-Cholesterol	3.1 ± 0.3	1.3 ± 0.4	0.94	1.15
7,7-d_2-Cholesterol	3.3 ± 0.2	1.6 ± 0.3		

P450 Spectra under Steady-state Reaction Conditions—One approach to discerning what step(s) in a P450 reaction is rate-limiting is to record UV-visible spectra in the steady-state reaction and observe which electronic state of P450 is domi-

[5] The experiments done in the absence of the reductase (photochemical reduction) did show a kinetic isotope effect, but this system was considered less relevant to the normal reaction (and had a much lower yield).

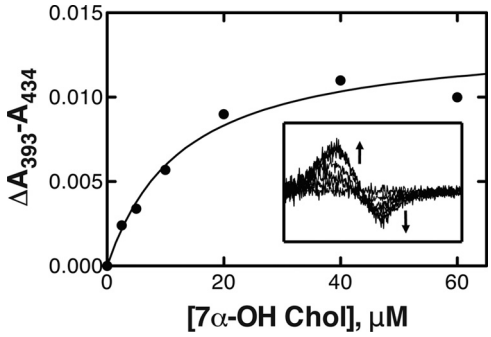

FIGURE 9. **Equilibrium binding of 7α-OH cholesterol to P450 7A1.** Titration of 1.0 μM P450 7A1 with increasing concentrations of 7α-OH cholesterol in the presence of 3.1 mM HPβCD and 0.41 mM Tween 20. The plot (*solid line*) is a fit result of the changes in absorbance (●) using the program Dynafit. An *inset* shows the spectral changes. Parameters: $K_1 = 2.5 \times 10^{-3}$ M, $K_2 = 1.5 \times 10^{-3}$ M, $K_3 = 3.7 \pm 0.4 \times 10^{-6}$ M. See supplemental Fig. S4 regarding fitting.

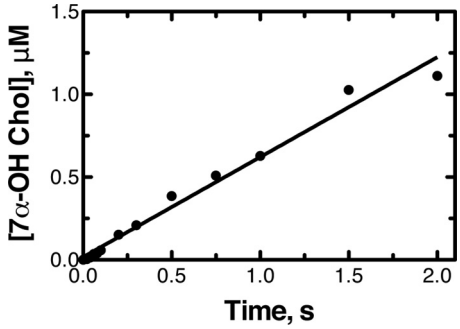

FIGURE 10. **Lack of burst kinetics in P450 7A1-catalyzed cholesterol 7α-hydroxylation.** The P450 7A1 concentration was 0.5 μM. The resulting data points were fit to a linear regression plot (GraphPad Prism).

TABLE 2

Yields of products formed from cholesterol in limited cycle experiments

System	Substrate	d_0-7α-OH cholesterol	d_1-7α-OH cholesterol	Theoretical yield
		nmol		*%*
P450 7A1 (hν[a])	d_0-Cholesterol	0.13		5.0[b]
	d_2-Cholesterol		0.024	1.0[c]
P450 7A1, reductase (NADPH)	d_0-Cholesterol	1.1		11[d]
	d_2-Cholesterol		0.96	9.6[e]

[a] Photochemical reduction.
[b] Yield = 0.13 nmol of d_0-7α-OH cholesterol/5 nmol of P450, × 2 (correction for $2e^-$ needed) = 0.05.
[c] Yield = 0.024 nmol of d_1-7α-OH cholesterol/5 nmol of P450, × 2 (correction for $2e^-$ needed) = 0.01.
[d] Yield = 1.1 nmol of d_0-7α-OH cholesterol/(5 nmol of P450 + 5 nmol of NADPH-P450 reductase + 12.5 nmol of NADPH) = 1.1 nmol of d_0-7α-OH cholesterol/10 nmol of reducing equivalents = 0.11.
[e] Yield = 0.96 nmol of d_1-7α-OH cholesterol/(5 nmol of P450 + 5 nmol of NADPH-P450 reductase + 12.5 nmol of NADPH) = 0.96 nmol of d_1-7α-OH cholesterol/10 nmol of reducing equivalents = 0.096.

TABLE 3

NADPH oxidation, product formation, and H_2O_2 formation by P450 7A1

Substrate	Rate			
	NADPH oxidation	7α-OH cholesterol formation	H_2O_2 formation	H_2O formation[a]
	nmol of product formed/min/nmol of P450 ± S.D. (n = 3)			
20 μM Cholesterol	179 ± 49	117 ± 6	44 ± 7	9

[a] Calculated by difference (38).

nant (16, 17, 39). We performed such an experiment in this case (Fig. 11). Because a high P450 concentration was required to observe spectra and the cholesterol 7α-hydroxylation is very rapid, we used the rapid-scanning mode of the stopped-flow spectrophotometer.

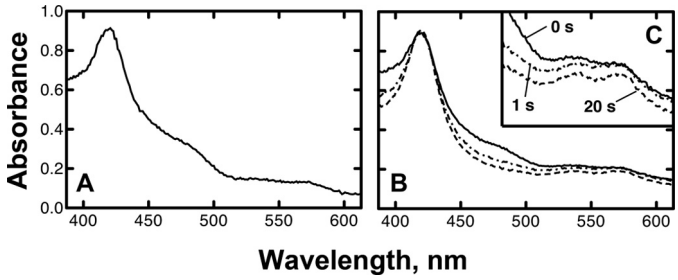

FIGURE 11. **Spectra of P450 7A1 during steady-state turnover.** One syringe of the stopped-flow spectrophotometer contained 6 μM P450 7A1, 12 μM NADPH-P450 reductase, 120 μM di-12:0 GPC, 40 μM cholesterol, 3.1 mM HPβCD, and 0.41 mM Tween 20 in 50 mM potassium phosphate buffer (pH 7.4), and the other syringe contained either air-saturated 50 mM potassium phosphate buffer (pH 7.4) including 3.1 mM HPβCD and 0.41 mM Tween 20 (*A*) or air-saturated 50 mM potassium phosphate buffer (pH 7.4) including 50 mM NADPH, 5 mM glucose 6-phosphate, 1 IU/ml yeast glucose 6-phosphate dehydrogenase, 3.1 mM HPβCD, and 0.41 mM Tween 20 (*B*). *A*, shown is a spectrum of P450 7A1 after mixing with air-saturated buffer (t = 20 s). *B*, shown are spectra of P450 7A1 after mixing with NADPH solution (*solid line*, *t* = 0 s; *dots and dashes*, 1 s; *dashed line*, 20 s). *C*, the *inset* shows an expansion of the heme α,β region. The spectral changes are uncorrected for the changes in the flavin spectra in *B* and *C*.

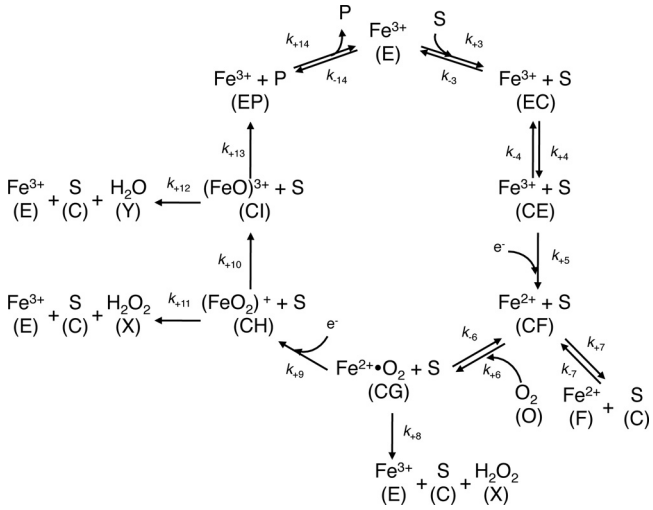

FIGURE 12. **Scheme used for kinetic modeling of cholesterol 7α-hydroxylation.** The scheme was used in the analysis (Table 4). *A*, Tween 20. *B*, HPβCD. *C*, cholesterol. *E*, P450 7A1 Fe^{3+}. *F*, P450 7A1 Fe^{2+}. *G*, P450 7A1 Fe^{2+}-O_2. *H*, P450 7A1 $(FeO_2)^+$. *I*, P450 7A1 $(FeO)^{3+}$. *O*, O_2. *P*, 7α-OH cholesterol. *X*, H_2O_2. *Y*, H_2O.

Although some changes between Fig. 11 *A* and *B* were observed (mainly due to the reduction of the flavins of the NADPH-P450 reductase), the magnitude of the Soret band and the characteristic α,β-band doublet were preserved in the steady-state spectra, as seen in the 1- and 20-s spectra (see supplemental Fig. S2 for comparisons of the Fe^{3+} and Fe^{2+} forms; the steady-state spectra are also not consistent with the spectra expected for the FeO_2^{2+} complex, based on other work; *i.e.* Fig. 7).

Kinetic Modeling—All steps shown in the general P450 reaction cycle (Fig. 1) were incorporated into a minimal kinetic model for the cholesterol 7α-hydroxylation reaction (Fig. 12). The model included the following phenomena: (i) the two-step binding of substrate to ferric P450 (Figs. 3, 4), (ii) irreversible decomposition of the ferrous P450-O_2-substrate

TABLE 4

Individual rate constants for P450 7A1 turnover

A, Tween 20; B, HPβCD; C, cholesterol; E, P450 7A1 Fe^{3+}; F, P450 7A1 Fe^{2+}; G, P450 7A1 $Fe^{2+}\dot{Y}O_2$; H, P450 7A1 $(FeO_2)^+$; I, P450 7A1 $(FeO)^{3+}$; O, O_2; P, 7α-OH cholesterol; X, H_2O_2; Y, H_2O.

Mechanism step	Forward rate constant	Reverse rate constant
C + A ⇄ CA	$k_{+1} = 1.0 \times 10^8$ M^{-1} s^{-1}	$k_{-1} = 2.5 \times 10^5$ s^{-1}
C + B ⇄ CB	$k_{+2} = 1.0 \times 10^8$ M^{-1} s^{-1}	$k_{-2} = 1.5 \times 10^5$ s^{-1}
C + E ⇄ EC	$k_{+3} = 2.5 \times 10^7$ M^{-1} s^{-1}	$k_{-3} = 98$ s^{-1}
EC ⇄ CE	$k_{+4} = 18.3$ s^{-1}	$k_{-4} = 2.4$ s^{-1}
CE → CF	$k_{+5} = 9.9$ s^{-1}	
CF + O ⇄ CG	$k_{+6} = 2.9 \times 10^5$ M^{-1} s^{-1}	$k_{-6} = 1$ s^{-1}
CF ⇄ F + C	$k_{+7} = 0.3$ s^{-1}	$k_{-7} = 1.9 \times 10^6$ M^{-1} s^{-1}
CG → E + C + X	$k_{+8} = 1.2$ s^{-1}	
CG → CH	$k_{+9} = 40$ s^{-1}	
CH → CI	$k_{+10} \geq 100$ s^{-1}	
CH → E + C + X	$k_{+11} = 25$ s^{-1}	
CI → E + C + Y	$k_{+12} = 5$ s^{-1}	
CI → EP	$k_{+13} \geq 100$ s^{-1}	
EP ⇄ E + P	$k_{+14} = 275$ s^{-1}	$k_{-14} = 2.5 \times 10^7$ M^{-1} s^{-1}

complex, (iii) irreversible loss of reduced oxygen species from the activated complex (O_2^-, H_2O_2, H_2O), (iv) the lack of burst kinetics (Fig. 10), (v) the lack of a non-competitive kinetic deuterium isotope effect (Fig. 8 and Table 1), and (vi) the low kinetic deuterium isotope effect when the reaction was started from the ferrous P450-substrate complex (Table 2).

The program Dynafit was used to fit plots of 7α-OH cholesterol, H_2O_2, and H_2O formation rates (single concentration points were used in the cases of the two reduced oxygen species) (supplemental Fig. S3*D*). The rate constants for cholesterol binding to ferric P450 (k_{+3}, k_{-3}, k_{+4}, and k_{-4}; Figs. 3 and 4), the first electron transfer (k_{+5}, Fig. 5), cholesterol binding to ferrous P450 (k_{+7} and k_{-7}, Fig. 6), and the decomposition of the ferrous P450-O_2-substrate complex (k_{+8}, Fig. 7) were used directly from the estimated rates obtained with experimental data.

In the modeling, a k_{-6} value of 1 s^{-1} was assumed to keep the k_{+6}/k_{-6} value in the low micromolar range (40). An estimate of k_{+6} was calculated by dividing the formation rate constant for the ferrous P450-O_2-cholesterol complex (Fig. 7*B*) by the O_2 concentration, 100 μM. The values of k_{+9} (the second electron transfer), k_{+10} (oxygen activation), k_{+11} (formation of H_2O_2 from the activated complex), k_{+12} (formation of H_2O from the activated complex), and k_{+13} (the C-H bond breaking) were estimated by fitting plots of the data. k_{+10} and k_{+13} were set as ≥100 s^{-1} for fitting. The value of k_{-14} (k_{on} for product binding) was optimized at 2.5×10^7 M^{-1} s^{-1} (Table 4) and could not be decreased without compromising the fit to the data. Using a K_d of 3.7 μM for 7α-OH cholesterol binding to P450 7A1 (Fig. 9), a value for k_{+14} was calculated.

The final fits for 7α-OH cholesterol, H_2O_2, and H_2O formation are shown in Fig. 13 using the rate constants presented in Table 4. The predicted curves of product formation rates fit the experimental data well without changing any of the rate constants estimated using the experimental results. Among the forward rate constants in the P450 reaction cycle producing 7α-OH cholesterol (*i.e.* k_{+3}, k_{+4}, k_{+5}, k_{+6}, k_{+9}, k_{+10}, k_{+13}, and k_{+14}), the first electron transfer rate constant (k_{+5}) showed the smallest value.

Kinetic Deuterium Isotope Effects on Cholesterol 7α-Hydroxylation Activity in Human Liver Microsomes—Human liver microsomes contain endogenous cholesterol (12). Cholesterol 7α-hydroxylation activity was measured in individual human liver microsomal samples using the endogenous cholesterol as substrate, adjusting the concentration of cholesterol to 20 μM by dilution (Table 5).

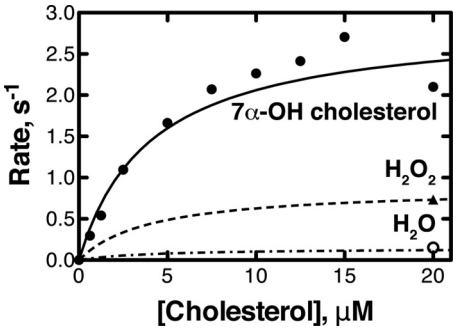

FIGURE 13. **Fitting of data for cholesterol 7α-hydroxylation and H_2O_2 and H_2O formation rates to the kinetic model.** The values of the rate constants used are those in Table 4. See supplemental Fig. S4 regarding fitting.

TABLE 5

Cholesterol 7α-hydroxylation activity in human liver (HL) microsomes

Human liver microsomes, sample number	Cholesterol	P450 7A1[a]	7α-Hydroxylation activity	7α-Hydroxylation activity
	nmol/mg microsomal protein	*pmol/mg microsomal protein*	*pmol/min/mg microsomal protein*	*nmol/min/nmol P450 7A1*
HL39	91	0.78	1.2	1.6
HL97	41	1.64	2.8	1.7
HL98	66	1.84	1.5	0.8
HL100	55	1.59	2.3	1.5
HL103	86	1.78	3.3	1.9
HL109	47	2.54	2.7	1.1
HL112	45	1.77	1.6	0.9
HL132	35	1.75	1.7	1.0
HL135	57	1.75	1.2	0.7
HL140	38	2.10	6.7	3.2
Average	56 ± 20	1.75 ± 0.44	2.5 ± 1.6	1.4 ± 0.7

[a] Immunoblot analysis, quantified based on the Fe^{2+}-CO *versus* Fe^{2+} difference spectrum of purified P450 7A1 using human P450 7A1 antibody (ab79847, Abcam).

The amount of P450 7A1 in each liver sample was estimated by immunoblotting and varied ~3-fold among the 10 liver samples examined. The catalytic activity (per nmol P450 7A1) varied ~5-fold, from 0.66 to 3.2 nmol of product formed/min/nmol of P450 7A1. The mean value, 1.4 min^{-1} (0.023 s^{-1}), was <1/100 the rate measured in the reconstituted system (Fig. 2).

Competitive deuterium isotope effects were also examined by changing the percentage of d_2-cholesterol in the total cholesterol concentration (100 μM). The percentage of d_1-7α-OH cholesterol formed increased linearly with the increase of the percentage of d_2-cholesterol used as substrate, with a slope of 1.1 (Fig. 14). This result indicates a lack of a kinetic deuterium isotope effect on 7α-hydroxylation activity in human liver microsomes.

DISCUSSION

The purpose of this study was to characterize the individual steps involved in cholesterol 7α-hydroxylation, a reaction catalyzed by P450 7A1 at a much higher rate than those of other mammalian P450s. The catalytic efficiency of the reaction is ~2.4×10^6 M^{-1} s^{-1} (Fig. 2), which can be compared with a typical P450 1A2 reaction, phenacetin *O*-deethylation at 2.3 ×

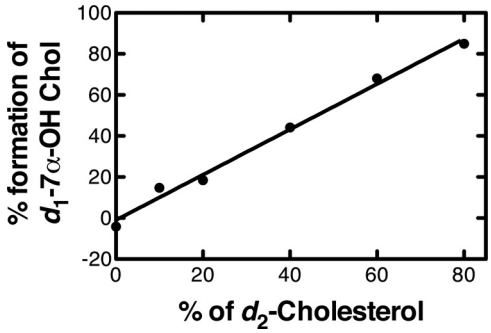

FIGURE 14. **Lack of kinetic deuterium isotope effect on cholesterol 7α-hydroxylation activity in human liver microsomes.** The resulting data points were fit to a linear regression plot (GraphPad Prism).

10^3 M^{-1} s^{-1}, and even the relatively efficient P450 3A4 testosterone 6β-hydroxylation reaction at 5.7×10^4 M^{-1} s^{-1} (15, 41). Previous reports on the low efficiency reactions of P450s 1A2, 2A6, 2D6, and 3A4 indicate that the C-H bond breaking step of each reaction is mainly or partially rate-limiting, as judged by kinetic deuterium isotope effects (15–18). Our results revealed that the substrate binding, C-H bond breaking, and product release steps are not rate-limiting and suggest that the first electron transfer step is the rate-limiting step in this high efficiency reaction. Although some of the older literature suggest that rate-limiting first-electron transfer is a general case (42, 43), the evidence argues against this view for most mammalian P450s in that high non-competitive kinetic deuterium isotope effects are rather common (15–18). In both early work with rat liver microsomes (42, 43) and later work with human liver microsomes (44), the rate of the fast phase of reduction of (total) P450 was ~0.7 s^{-1} (41 min^{-1}). This rate is considerably higher than the rates of most P450-catalyzed oxidations of xenobiotic chemicals.

In our experimental conditions using reconstituted systems containing purified P450 7A1 and NADPH-P450 reductase, we used Tween 20 and HPβCD for delivering the substrate cholesterol and obtained high catalytic activities for P450 7A1 (Fig. 2*A*). Cholesterol binds to both Tween 20 and HPβCD (45). Thus, all models used to fit the data in this report included two additional steps (*i.e.* cholesterol + Tween 20 ⇄ cholesterol-Tween 20 and cholesterol + HPβCD ⇄ cholesterol-HPβCD). The kinetic traces of spectral changes of P450 7A1 followed by binding of cholesterol could be well fit to a two-step binding model (E + L ⇄ EL ⇄ LE), with a K_d value of 0.51 μM, as shown previously with some other P450s (Fig. 4, supplemental Fig. S5) (33–35). Interestingly, when the lipid (di-12:0 GPC) was removed from the reaction mixture, the observed rates (k_{obs}) were >3-fold lower than those with di-12:0 GPC (results not shown). A previous report indicated the importance of some amino acid residues in the membrane binding domain of P450 7A1 for cholesterol binding and substrate specificity (9). Our results also suggest that the interaction between P450 7A1 and a lipid membrane is important for rapid binding of cholesterol.

A rapid reduction rate was obtained in the presence of cholesterol, although only ~60% of the P450 7A1 was reduced in the fast phase (9.9 s^{-1} at 37 °C) (Fig. 5, supplemental Fig. S4*C*). This reduction rate was comparable with those of several other mammalian P450s (16, 17, 33, 44).

The catalytic efficiency of a reaction can be expressed as the second-order rate constant for binding multiplied by the efficiency of productive catalytic events. The efficiency here is high (2.4×10^6 M^{-1} s^{-1}, Fig. 2*A*) but the reaction is clearly not diffusion-limited, as shown by the evidence against substrate binding being rate-limiting (Fig. 10).

The work on kinetic deuterium isotope effects was done with 7,7-d_2-cholesterol. We did not utilize the individually labeled 7-*d* isomers (7α, 7β) in our work. However, *in vivo* studies with rats by Corey and Gregoriou (46) and Bergstrom *et al.* (26) have shown that only the 7α-hydrogen atom is abstracted. We presume that the same course is probably followed in humans, *i.e.* that hydrogen abstraction and oxygen rebound both occur from the α-face. The potential for a contributing geminal secondary kinetic deuterium isotope effect (due to the use of 7,7-d_2-cholesterol) in our work is not an issue, in that no isotope effects were observed (Table 1, Fig. 8).

The lack of a kinetic deuterium isotope effect (Fig. 8) and kinetic burst when the reaction cycle was initiated from the ferric P450 7A1-cholesterol complex (Fig. 10) clearly shows that the substrate binding, C-H bond breaking, and product-release steps are not rate-limiting. Therefore, we considered the possibility that the rate-limiting step could be the first electron transfer. The deuterium isotope effect was measured in an experiment in which the reaction cycle was started from the ferrous P450 7A1-cholesterol complex, namely just after the first electron transfer (Table 2). No kinetic isotope effect was observed, indicating that the C-H bond breaking step is faster than the rates of O_2 binding, the second electron transfer, and the O_2 activation steps (Fig. 1).

A minimal kinetic model (Fig. 12, supplemental Fig. S4*D*) for the cholesterol 7α-hydroxylation reaction was developed, including all steps shown in the general P450 reaction (Fig. 1). The predicted progress curves for 7α-OH cholesterol, H_2O_2, and H_2O formation fit the experimental data well without changing any of the rate constants estimated using the experimental results (Fig. 13, Table 4). The value of k_{+13} (C-H bond breaking) was greater than those of k_{+6} (O_2 binding to ferrous P450-cholesterol complex), k_{+9} (the second electron transfer), and k_{+10} (oxygen activation), consistent with the kinetic deuterium isotope effect results in the limited turnover experiment. The ratio of k_{+13} and k_{+12} was comparable with the ratio of the 7α-OH cholesterol and H_2O formation rates (Tables 3 and 4). Among the forward rate constants in the P450 reaction cycle producing 7α-OH cholesterol (*i.e.* k_{+3}, k_{+4}, k_{+5}, k_{+6}, k_{+9}, k_{+10}, k_{+13}, and k_{+14}), the first electron transfer rate constant (k_{+5}) showed the smallest value. These results indicate that the first electron transfer step is rate-limiting. However, a more appropriate view of the catalytic cycle is not to conclude that a single step is rate-limiting but that the overall reaction rate reflects the contribution of rate constants of back reactions and side reactions (47).

A typical ratio of NADPH-P450 reductase and P450 in reconstituted P450 systems is ~2:1 for maximum catalytic activity (16, 17, 48, 49). However, the ratios of NADPH-P450

reductase and P450 7A1 (50:1 for steady-state enzyme kinetic work and 15:1 for burst kinetic analysis) used in this report were much higher (Fig. 2*B*), consistent with our conclusion that the rate of reduction limits the overall reaction both in the reconstituted system and in microsomal membranes. For other mammalian P450s the C-H bond breaking step is often rate-limiting in steady-state turnover (16, 17), and the "saturation" of a P450 by NADPH-P450 reductase leads to an approach to a limiting steady-state rate (imposed by the C-H bond breaking step). On the other hand, the increase of the reduction capacity in the reaction system enhances the catalytic activity of P450 7A1 because the rate-limiting step of the P450 7A1 reaction may be the first electron transfer step.

Competitive kinetic deuterium isotope effect experiments on cholesterol 7α-hydroxylation activity were also conducted in human liver microsomes. The ratio of the total amounts of P450 and NADPH-P450 reductase in human liver microsomes has been reported to be ~20:1 (50). If the rate-limiting step in the cholesterol 7α-hydroxylation reaction is the first electron transfer step, then no isotope effect should be observed due to the very limited capacity for reduction in human liver microsomes. The percentage of formation of (7β-d_1)7α-OH cholesterol increased proportionately with the increase of the percentage of d_2-cholesterol added, with a slope of 1.1 (Fig. 13), indicating the lack of an isotope effect on 7α-hydroxylation activity in human liver microsomes. This result supports the proposal that the rate-limiting step is the first electron transfer step in the microsomal membranes as well as the reconstituted system. The high catalytic efficiency of P450 7A1, once reduced, is consistent with evidence for high binding selectivity for cholesterol in the mode for 7α-hydroxylation (45), leaving the rate of the reaction dependent upon reduction (Fig. 2*B*). However, it was noted (45) that even this fit is precarious in that the P450 7A1 mutant A358V formed 7β-OH cholesterol and an unidentified product, and we have recently determined that 7-dehydrocholesterol, the immediate precursor of cholesterol, is also a substrate for P450 7A1.[6]

In summary, we evaluated the kinetic mechanism of human P450 7A1-catalyzed cholesterol 7α-hydroxylation, measuring rate constants of individual steps and kinetic deuterium isotope effects. A minimal kinetic model for the P450 7A1 reaction indicates that the first electron transfer step is rate-limiting and that this is a clearly different phenomenon compared with other P450s that have much lower rates of catalysis.

Acknowledgments—We thank M. V. Martin and L. M. Folkmann for preparation of NADPH-P450 reductase, I. A. Pikuleva for the P450 7A1 plasmid, M. W. Calcutt for technical assistance with MS analyses, and K. Trisler for help in preparation of the manuscript.

REFERENCES

1. Northrop, D. B. (1975) *Biochemistry* **14,** 2644–2651
2. Northrop, D. B. (1982) *Methods Enzymol.* **87,** 607–625
3. Guengerich, F. P. (2001) *Chem. Res. Toxicol.* **14,** 611–650
4. Ortiz de Montellano, P. R., and De Voss, J. J. (2005) in *Cytochrome P450: Structure, Mechanism, and Biochemistry* (Ortiz de Montellano, P. R., ed.) 3rd Ed., pp. 183–245, Plenum Publishers, New York
5. Sligar, S. G., Makris, T. M., and Denisov, I. G. (2005) *Biochem. Biophys. Res. Commun.* **338,** 346–354
6. Loughran, P. A., Roman, L. J., Aitken, A. E., Miller, R. T., and Masters, B. S. S. (2000) *Biochemistry* **39,** 15110–15120
7. Guengerich, F. P., Dannan, G. A., Wright, S. T., Martin, M. V., and Kaminsky, L. S. (1982) *Biochemistry* **21,** 6019–6030
8. Dierks, E. A., Davis, S. C., and Ortiz de Montellano, P. R. (1998) *Biochemistry* **37,** 1839–1847
9. Nakayama, K., Puchkaev, A., and Pikuleva, I. A. (2001) *J. Biol. Chem.* **276,** 31459–31465
10. Pikuleva, I. A. (2006) *Pharmacol. Ther.* **112,** 761–773
11. Russell, D. W., and Setchell, K. D. (1992) *Biochemistry* **31,** 4737–4749
12. Einarsson, K., Reihnér, E., and Björkhem, I. (1989) *J. Lipid Res.* **30,** 1477–1481
13. Martin, K. O., Budai, K., and Javitt, N. B. (1993) *J. Lipid Res.* **34,** 581–588
14. Maeda, Y. R., Eggertsen, G., Nyberg, B., Setoguchi, T., Okuda, K. I., Einarsson, K., and Björkhem, I. (1995) *Eur. J. Biochem.* **228,** 144–148
15. Krauser, J. A., and Guengerich, F. P. (2005) *J. Biol. Chem.* **280,** 19496–19506
16. Guengerich, F. P., Krauser, J. A., and Johnson, W. W. (2004) *Biochemistry* **43,** 10775–10788
17. Yun, C. H., Kim, K. H., Calcutt, M. W., and Guengerich, F. P. (2005) *J. Biol. Chem.* **280,** 12279–12291
18. Guengerich, F. P., Miller, G. P., Hanna, I. H., Sato, H., and Martin, M. V. (2002) *J. Biol. Chem.* **277,** 33711–33719
19. Hanna, I. H., Teiber, J. F., Kokones, K. L., and Hollenberg, P. F. (1998) *Arch. Biochem. Biophys.* **350,** 324–332
20. Cunningham, I. M., and Overton, K. H. (1974) *J. Chem. Soc. Perkin 1,* 2458–2462
21. Wilson, W. K., Sumpter, R. M., Warren, J. J., Rogers, P. S., Ruan, B., and Schroepfer, G. J., Jr. (1996) *J. Lipid Res.* **37,** 1529–1555
22. Brunel, J. M., Billottet, l., and Letourneux, Y. (2005) *Tetrahedron Assymmetry* **16,** 3036–3041
23. Guengerich, F. P., and Bartleson, C. J. (2007) in *Principles and Methods of Toxicology* (Hayes, A. W., ed) 5th Ed., pp. 1981–2048, CRC Press, Boca Raton, FL
24. Tang, Z., and Guengerich, F. P. (2010) *Anal. Chem.* **82,** 7706–7712
25. Kuzmic, P. (1996) *Anal. Biochem.* **237,** 260–273
26. Bergstrom, S., Lindstredt, S., Samuelson, B., Corey, E. J., and Gregprious, G. A. (1958) *J. Am. Chem. Soc.* **80,** 2337–2338
27. Patil, P. V., and Ballou, D. P. (2000) *Anal. Biochem.* **286,** 187–192
28. Johnson, K. A., Simpson, Z. B., and Blom, T. (2009) *Anal. Biochem.* **387,** 20–29
29. Mast, N., and Pikuleva, I. A. (2005) *J. Lipid Res.* **46,** 1561–1568
30. Norlin, M., Andersson, U., Björkhem, I., and Wikvall, K. (2000) *J. Biol. Chem.* **275,** 34046–34053
31. Schenkman, J. B., Remmer, H., and Estabrook, R. W. (1967) *Mol. Pharmacol.* **3,** 113–123
32. Fersht, A. (1999) *Structure and Mechanism in Protein Science*, pp. 158–159, W. H. Freeman and Co., New York
33. Sohl, C. D., and Guengerich, F. P. (2010) *J. Biol. Chem.* **285,** 17734–17743
34. Sohl, C. D., Isin, E. M., Eoff, R. L., Marsch, G. A., Stec, D. F., and Guengerich, F. P. (2008) *J. Biol. Chem.* **283,** 7293–7308
35. Isin, E. M., and Guengerich, F. P. (2007) *J. Biol. Chem.* **282,** 6863–6874
36. Oprian, D. D., Gorsky, L. D., and Coon, M. J. (1983) *J. Biol. Chem.* **258,** 8684–8691
37. Denisov, I. G., Grinkova, Y. V., Baas, B. J., and Sligar, S. G. (2006) *J. Biol. Chem.* **281,** 23313–23318
38. Gorsky, L. D., Koop, D. R., and Coon, M. J. (1984) *J. Biol. Chem.* **259,** 6812–6817
39. Yamazaki, H., Ueng, Y. F., Shimada, T., and Guengerich, F. P. (1995) *Biochemistry* **34,** 8380–8389
40. Mueller, E. J., Loida, P. J., and Sligar, S. G. (1995) in *Cytochrome P450:*

[6] R. Shinkyo, L. Xu, N. A. Porter, and F. P. Guengerich, unpublished information.

Structure, Mechanism, and Biochemistry (Ortiz de Montellano, P. R., ed) 2nd Ed., pp. 83–124, Plenum Publishers, New York,
41. Yun, C. H., Miller, G. P., and Guengerich, F. P. (2000) *Biochemistry* **39,** 11319–11329
42. Gigon, P. L., Gram, T. E., and Gillette, J. R. (1969) *Mol. Pharmacol.* **5,** 109–122
43. Diehl, H., Schädelin, J., and Ullrich, V. (1970) *Hoppe-Seyler's Z. Physiol. Chem.* **351,** 1359–1371
44. Guengerich, F. P., and Johnson, W. W. (1997) *Biochemistry* **36,** 14741–14750
45. Mast, N., Graham, S. E., Andersson, U., Bjorkhem, I., Hill, C., Peterson, J., and Pikuleva, I. A. (2005) *Biochemistry* **44,** 3259–3271
46. Corey, E. J., and Gregoriou, G. A. (1959) *J. Am. Chem. Soc.* **81,** 3127–3133
47. Johnson, K. A. (2008) *J. Biol. Chem.* **283,** 26297–26301
48. Shaw, P. M., Hosea, N. A., Thompson, D. V., Lenius, J. M., and Guengerich, F. P. (1997) *Arch. Biochem. Biophys.* **348,** 107–115
49. Yamazaki, H., Nakano, M., Gillam, E. M., Bell, L. C., Guengerich, F. P., and Shimada, T. (1996) *Biochem. Pharmacol.* **52,** 301–309
50. Estabrook, R. W., Franklin, M. R., Cohen, B., Shigamatzu, A., and Hildebrandt, A. G. (1971) *Metabolism* **20,** 187–199